PFC/JA-94-38

X-ray Observations of $2l$ - nl' Transitions in Mo^{30+} - Mo^{33+} from Tokamak Plasmas

J.E. Rice, K.B. Fournier[1], M.A. Graf, J.L. Terry,
M. Finkenthal[2], F. Bombarda[3], E.S. Marmar, W.H. Goldstein[1]

Plasma Fusion Center
Massachusetts Institute of Technology
Cambridge, MA 02139

November, 1994

[1]Lawrence Livermore National Laboratory, Livermore, CA.
[2]Johns Hopkins University, Baltimore, MD.
[3]ENEA-Frascati, Frascati, Italy.

Submitted to Phys. Rev. A.

This work was supported by the U. S. Department of Energy Contract No. DE-AC02-78ET51013. Reproduction, translation, publication, use and disposal, in whole or in part by or for the United States government is permitted.

X-ray Observations of $2l$ - nl' Transitions in Mo^{30+} - Mo^{33+} from Tokamak Plasmas

J. E. Rice, K. B. Fournier[+], M. A. Graf, J. L. Terry, M. Finkenthal[!], F. Bombarda[*], E. S. Marmar and W. H. Goldstein[+]

Plasma Fusion Center, MIT

Cambridge, MA 02139-4307

[+] *Lawrence Livermore National Laboratory, Livermore, CA*

[!] *Johns-Hopkins University, Baltimore, MD*

[*] *Associazione ENEA-Euratom per la Fusione, 00044 Frascati, Italy*

Abstract

X-ray spectra of 2p - nd transitions with $4 \leq n \leq 13$ in molybdenum (Z=42) charge states around neon-like (Mo^{32+}) have been observed from Alcator C-Mod plasmas. Accurate wavelengths ($\pm$ .1 mÅ) have been determined by comparison with neighboring argon and chlorine lines with well known wavelengths. Line identifications have been made by comparison to *ab initio* atomic structure calculations, using a fully relativistic, parametric potential code, and agreement between measured and theoretical wavelengths is good. Calculated wavelengths and oscillator strengths are presented for all transitions with upper levels n between 4 and 14 to the lower levels $n = 2$ in the four charge states Mo^{30+} - Mo^{33+}. Effects of configuration interaction has been observed in the intensities of lines with nearly degenerate energy levels.

Introduction

The soft x-ray spectrum of molybdenum has been studied extensively in tokamak, laser and pulsed-power produced plasmas. In tokamaks, the abundance and spatial distribution of the various charge states affect the power balance of the plasma and may influence the current density profile, particle transport and plasma resistivity[1,2]. In laser produced plasmas, x-ray energy conversion efficiencies have been studied using molybdenum targets irradiated by high power visible lasers[3]. These sources have also been used for emission spectroscopy studies of the 3-3, 2-2, 2-3 and 2-4 transitions of the charge states around neon-like[4–7]. Theoretical energy level computations have been limited mainly to these transitions[8,9]. Transitions between highly excited states and ground or near-ground states have not been reported in the past. In high density (laser and pulsed-power) plasmas, these levels may be depopulated by collisions; in high temperature, low density ($10^{20}/m^3$) tokamak plasmas such measurements are possible. Besides the purely spectroscopic interest in these transitions (line classifications and comparison with *ab initio* atomic structure calculations), these lines are good candidates to benchmark the collisional-radiative models used in power loss estimates, because of their great temperature sensitivity.

In spite of the deleterious effect of large concentrations of high Z materials on fusion plasmas, they will have to be used in the walls and various structural components of future fusion reactors. The Alcator C-Mod tokamak[10] has all molybdenum plasma facing components and one of the main thrusts of the present experiments on this device is the study of the impurity production and the screening of the core plasma by means of the divertor configuration[11]. This provides the opportunity for the detailed study of molybdenum charge states around the neon-like iso-sequence. The $\Delta n = 1$ x-ray transitions from these charge states have previously been studied from Alcator A[12] and Alcator C[13]. $\Delta n \geq 1$ transitions have been obtained from exploding wires[14], but the wavelength resolution was low.

In the present paper, high resolution x-ray observations (2.97 Å$\leq \lambda \leq$ 3.84 Å) of $2 \leq \Delta n \leq 11$ transitions from Mo^{31+}, Mo^{32+} and Mo^{33+} will be presented. For

these measurements, the plasma parameters were in the range of 1.2 x $10^{20}/m^3 \leq n_{e0} \leq 2.0$ x $10^{20}/m^3$ and 1500 eV $\leq T_{e0} \leq$ 2100 eV.

Instrument Description and Calibration Method

A five chord, independently spatially scannable, high resolution x-ray spectrometer array[15] has been installed on the Alcator C-Mod tokamak. Each von Hamos type spectrometer consists of a variable entrance slit, a quartz crystal (2d=6.687 Å) and a position sensitive proportional counter detector. Each spectrometer has a resolving power of 4000, a 3 cm spatial resolution and a wavelength range of 2.8 to 4.0 Å. Spectra are typically collected every 50 ms during a discharge, with 120 mÅ covered at any one wavelength setting. A typical value of the spectrometer luminosity function is 7 x 10^{-13} m^2sr, calculated from the crystal reflectivity, spectrometer geometry and Be window transmission. Wavelength calibration has been achieved by determining the instrumental dispersions from reference to argon and chlorine lines. The argon was introduced through a piezo-electric valve and chlorine is an intrinsic impurity from solvents used to clean vacuum components. Lines from hydrogen- and helium-like charge states are taken to have well known wavelengths, either measured or calculated. The transitions used in the current wavelength calibration are listed in Tables I and II, along with the appropriate references.

Calculation of Energy Levels and Oscillator Strengths

Ab initio atomic structure calculations for Mo^{29+} through Mo^{33+} (ground states $2p^63s^23p$ to $2s^22p^5$, respectively) have been performed using the HULLAC package developed at the Hebrew University and Lawrence Livermore National Laboratories. The HULLAC package produces atomic wave functions using the parametric potential code RELAC[21,22]. The package includes ANGLAR which uses the graphic angular recoupling program NJGRAF to generate fine structure levels in a j-j-coupling scheme for a set of user-specified electron configurations[23]. RELAC then calculates

energy levels in addition to radiative and auger[24,25] transition probabilities.

This paper reports the wavelengths and oscillator strengths for newly identified 2s-np, 2p-ns and 2p-nd transitions in highly ionized molybdenum. Full collisional-radiative models have been constructed using the CROSS suite of codes[26] in the HULLAC package to calculate the collisional excitation rate coefficients in the Distorted Wave Approximation between levels in a given ion. Accounting for excitation-autoionization processes to and from adjacent charge states, the collisional-radiative models revealed the x-ray transitions classified here to be the overwhelmingly dominant transitions in these ions.

The 2p-nd transitions considered here are found to be strongly split by the j-value of the 2p hole in the ionic core. The resonance transitions with upper states containing a $2p_{\frac{1}{2}}$ hole are always at much shorter wavelengths than the corresponding transitions with a $2p_{\frac{3}{2}}$ hole. This can lead to significant configuration interaction when a $2p_{\frac{1}{2}}nd$ orbital is close in energy to a $2p_{\frac{3}{2}}n'd$ (n'>n) orbital. Interaction between the orbitals will affect both transition rates and transition wavelengths[27]. Table III demonstrates the wave function mixing in Mo^{32+} for two cases where the degeneracy in energy makes the configuration interaction very strong. The energies of the $(2p^5)_{\frac{1}{2}}6d_{\frac{3}{2}}$ J=1 level and the $(2p^5)_{\frac{3}{2}}7d_{j'}$ J=1 levels are between 3946 and 3950 eV; the energies of the $(2p^5)_{\frac{3}{2}}6d_{j''}$ levels are down near 3830 eV and the $(2p^5)_{\frac{1}{2}}7d_{j'''}$ levels are near 4060 eV. As can be seen in Table III for the $(2p^5)_{\frac{1}{2}}6d_{\frac{3}{2}}$ J=1 level the near degeneracy in energy of the $(2p^5)_{\frac{3}{2}}7d_{j'}$ J=1 levels means a significant amount of the $(2p^5)_{\frac{1}{2}}6d_{\frac{3}{2}}$ J=1 wave function is made up of other orbitals from other configurations. This near degeneracy also exists for the $(2p^5)_{\frac{1}{2}}8d_{\frac{3}{2}}$ J=1 level and the $(2p^5)_{\frac{3}{2}}11d_{j'}$ J=1 levels. Similar configuration interaction effects are seen for Mo^{30+} between the $(2p^5)_{\frac{1}{2}}[3s^2]7d_{\frac{3}{2}}$ level and the $(2p^5)_{\frac{3}{2}}[3s^2]9d_{\frac{5}{2}}$ level (see Table IV), and for Mo^{31+} between the $(2p^5)_{\frac{1}{2}}[3s]8d_{\frac{3}{2}}$ $J = \frac{3}{2}$ level and the $(2p^5)_{\frac{3}{2}}[3s]11d_{\frac{5}{2}}$ $J = \frac{3}{2}$ level (see Table V). The effect is much stronger in Mo^{30+} where the levels are nearly degenerate. The physical implications of this phenomenon will be seen below.

Observed Molybdenum Spectra

Shown in Figure 1 is a spectrum between 3.7 and 3.8 Å, obtained from a plasma with an electron temperature of 1800 eV and an electron density of 1.7 x $10^{20}/m^3$. This shows the brightest molybdenum line that falls in the range of the spectrometer system, the $2p_{\frac{3}{2}}$ - $4d_{\frac{5}{2}}$ transition in Mo^{32+} at 3739.8 mÅ. The wavelength of this line has been determined by comparison to neighboring lines with accurately known wavelengths, in particular the Lyman α doublet of Ar^{17+}, nearby satellites and the $1s^2$-1s3p transition in Cl^{15+} (see Tables I and II). Both Mo^{32+} and Ar^{17+} are located in the plasma center and have the same ion temperature so the molybdenum line is narrower than the argon lines due to the lower thermal velocity. Similar transitions in sodium-like Mo^{31+} appear as an unresolved group centered at 3785.7 mÅ. Also apparent is a 2p-4d transition of magnesium-like Mo^{30+} at 3715.5 mÅ, although this line is quite weak. Other molybdenum lines in this spectrum are at 3717.8, 3759.1 and 3799.6 mÅ. Shown at the bottom of the figure are computed lines from neon-like, sodium-like and magnesium-like molybdenum, and from hydrogen-like argon and satellites, and helium-like chlorine. The wavelength agreement of the observed and calculated Mo^{32+} lines is excellent, fair (within .5 mÅ) for the Mo^{31+} lines and less than outstanding (off by 2.9 mÅ) for the Mo^{30+} lines.

Figure 2 shows a spectrum from 3.6 to 3.7 Å. Plasma parameters for which this spectrum was obtained were n_{e0} = 1.6 x $10^{20}/m^3$ and T_{e0} = 2100 eV. The strongest line in this spectral region is the $2p_{\frac{1}{2}}$ - $4d_{\frac{3}{2}}$ transition of Mo^{32+} at 3626.1 mÅ. Also visible are a pair of unresolved 2p-4d lines of Mo^{31+} at 3670.6 mÅ, and a 2p-4d line of fluorine-like Mo^{33+} at 3615.3 mÅ. There is also a pair of Mo^{33+} lines around 3604 mÅ, but these blend with the $1s^2$-1s4p transition of Cl^{15+} at 3603.56 mÅ. Shown at the bottom of the figure are theoretical lines from Mo^{32+}, Mo^{31+}, Mo^{33+} and Cl^{15+}. The wavelength agreement for the neon- and fluorine-like lines is quite good (within .2 mÅ). This a particularly interesting portion of the x-ray spectrum since three adjacent charge states are visible simultaneously, and models for ionization state balance may be tested. This will be the subject of a forthcoming

paper.

Continuing to higher n transitions, in Figure 3 is shown the spectrum in the vicinity of 3.4 Å, from a discharge with n_{e0} = 1.2 x $10^{20}/m^3$ and T_{e0} = 1500 eV. The brightest line is the $2p_{\frac{3}{2}}$ - $5d_{\frac{5}{2}}$ transition in Mo^{32+} at 3392.0 mÅ, and other 2p-5d transitions in sodium- and magnesium-like molybdenum are apparent. There are also two 2s-4p lines of Mo^{32+} at 3439.2 and 3450.7 mÅ. Also in this spectrum are Ar^{15+} satellites to the Ar^{16+} $1s^2$-1s3p line with n=2 spectators. The wavelength agreement is good (within .3 mÅ) for transitions with a 2p lower level, but those with the 2s lower level are off by 1.5 mÅ. The $2s2p^64p$ J=1 levels are well separated in energy from the levels of other configurations in this model with the same parity, so their wave functions are extremely pure. The accuracy of calculated transition wavelengths for radiative decays to an inner-shell hole is known to be worse than that for decays to a valence hole because of several factors. One problem comes from incomplete accounting of configuration interaction with doubly excited states. Although a significant problem for the $2s2p^6nl$ configurations in heavier elements, the lowest energy doubly excited configuration, $2s^22p^43s^2$, is over 1 keV away in energy in neon-like molybdenum. For neon-like charge states of heavier elements, observations[28] have shown that calculations consistently overestimate the self-energy contribution of the 2s hole to the 2s-np transitions. Finally, the calculations of the Lamb shift and the Breit interaction energy in RELAC are approximate and a discussion of their associated contributions to uncertainties in transition wavelengths can be found in Ref. (22).

The spectrum between 3.0 and 3.1 Å is shown in Figure 4. This was obtained from a series of several similar discharges with n_{e0} = 1.3 x $10^{20}/m^3$ and T_{e0} = 1600 eV. The Mo^{32+} series $2p_{\frac{3}{2}}$ - $nd_{\frac{5}{2}}$ with n = 8, 9, 10, 11, 12 and 13 can be seen, as well as the $2p_{\frac{1}{2}}$ - $7d_{\frac{3}{2}}$ (3054.9 mÅ) and $2p_{\frac{1}{2}}$ - $8d_{\frac{3}{2}}$ (unresolved from $2p_{\frac{3}{2}}$ - $11d_{\frac{5}{2}}$) transitions. Theoretical lines (solid) are shown at the bottom of the figure, and the wavelength agreement is excellent. Wavelength calibration was obtained by comparison to nearby Ar^{16+} ($1s^2$ - 1snp with $5 \leq n \leq 13$) lines[20,29] (see Table I).

Mo^{31+} (dotted) and Mo^{33+} (dashed) lines are also identified. The Mo^{32+} $2p_{\frac{5}{2}}$ - $13d_{\frac{3}{2}}$ line is considerably stronger than the $2p_{\frac{5}{2}}$ - $12d_{\frac{3}{2}}$ line. This could be because this line is at the edge of the detector, where there are potential distortions in the sensitivity. It could possibly be due to charge exchange recombination contributions to the population of the n = 13 level, from transfer between neutral hydrogen and Mo^{33+}. This should occur into levels[30] near $(32)^{3/4} = 13.5$.

Measured and theoretical wavelengths and differences, calculated gf values and line identifications are summarized in Tables IV-VII for the charge states Mo^{30+}-Mo^{33+}. Wavelength agreement is better than .5 mÅ in most cases. In Figures 1-4, the relative intensities of the theoretical lines from a given charge state are determined by the gf values from the tables. The gf values from the $2p_{\frac{3}{2}}$ - $nd_{\frac{5}{2}}$ and $2p_{\frac{1}{2}}$ - $nd_{\frac{3}{2}}$ series in Mo^{32+} are plotted as a function of n in Figure 5. Also shown are curves proportional to n^{-3} (the dependence for H-like ions at high n), which reflect the general trend. The $2p_{\frac{1}{2}}$ - $6d_{\frac{3}{2}}$ transition, however, is about a factor of three below this trend. This is supported by the observed line intensities. Shown in Figure 6 is a spectrum which includes the Mo^{32+} $2p_{\frac{3}{2}}$ - $7d_{\frac{5}{2}}$ transition at 3138.5 mÅ, as well as the Ar^{16+} $1s^2$ - 1s5p and Ar^{17+} 1s-3p lines used for the wavelength calibration (see Table I). There is also a feature at 3141.8 mÅ, which could be the Mo^{32+} $2p_{\frac{1}{2}}$ - $6d_{\frac{3}{2}}$ line (solid), or a Mo^{31+} 2p-8d line (dotted). The ratio of the two calculated Mo^{32+} gf values is 5.7, whereas the ratio from the two curves in Figure 5 for these lines is 1.2. From Figure 6 it is clear that the $2p_{\frac{3}{2}}$ - $7d_{\frac{5}{2}}$ line is much stronger than the $2p_{\frac{1}{2}}$ - $6d_{\frac{3}{2}}$ line (if it is even visible at all) consistent with the calculated gf values. The reason that the $2p_{\frac{1}{2}}$ - $6d_{\frac{3}{2}}$ line is so weak is because of the configuration interaction between the $(2p^5)_{\frac{1}{2}}6d_{\frac{3}{2}}$ J=1 state and the $(2p^5)_{\frac{3}{2}}7d_{j'}$ J=1 states that occurs due to their near degeneracy in energy. Similar effects have been observed and modelled in other tokamak plasmas[31]. The same effect is seen on the $2p_{\frac{1}{2}}$ - $8d_{\frac{3}{2}}$ gf value in Fig. 5; this value is also below the smooth curve. The $(2p^5)_{\frac{1}{2}}$ - $8d_{\frac{3}{2}}$ J=1 level interacts with the nearby $(2p^5)_{\frac{3}{2}}$ - $11d_{j'}$ J=1 levels. However, it is unresolved from the $2p_{\frac{3}{2}}$ - $11d_{\frac{5}{2}}$ transition so their relative intensities cannot be determined (see Fig. 4).

Conclusions

X-ray spectra of highly ionized molybdenum in the wavelength range from 2.97 - 3.84 Å have been obtained from the Alcator C-Mod tokamak. Wavelengths for 2p - nd transitions with $n \geq 4$ for neon-, sodium-, magnesium- and fluorine-like molybdenum have been determined by reference to nearby argon and chlorine lines, with an accuracy of $\pm$ 0.1 mÅ. Line identifications have been made by comparison to atomic structure calculations, using a fully relativistic, parametric potential code. The agreement between measured and theoretical wavelengths is quite good, with most lines within 0.5 mÅ. Effects of configuration interaction have been seen in the intensities of transitions with nearly degenerate energy levels.

Acknowledgements

The authors would like to thank K. Giesing for assistance with the data reduction, T. Luke for electron density measurements, A. Hubbard for electron temperature measurements and the Alcator C-Mod operations group for expert running of the tokamak. Work supported by DoE Contract No. DE-AC02-78ET51013

References

[1] R.C.Isler, Nucl. Fusion **24**, 1599 (1984)

[2] C.DeMichelis and M.Mattioli, Rep. Prog. Phys. **47**, 1233 (1984)

[3] G.M.Zeng et al., J. Appl. Phys. **72**, 3355 (1992)

[4] A.Wouters et al., J. Opt. Soc. Am. **B5**, 1520 (1988)

[5] C.Jupen et al., Phys. Scr. **41**, 669 (1990)

[6] B.K.F.Young et al., Phys. Rev. A **62**, 1266 (1989)

[7] V.A.Boiko et al., J. Phys. B **11**, 503 (1978)

[8] A.L.Gogava et al., Opt. Spectrosc. (USSR) **64**, 435 (1988)

[9] Y.K.Kim et al., Phys. Rev. A **44**, 148 (1991)

[10] I.H.Hutchinson et al., Phys. Plasmas **1**, 1511 (1994)

[11] F. Wagner and K Lackner in "Physics of Plasma Wall Interactions in Controlled Fusion" (Proc of NATO Advanced Study Institute, Val-Morin Quebec,1984), Ed D E Post and R Behrisch, NATO ASI Series, Vol **131**, Plenum Press, New York p. 931 (1986)

[12] J.E.Rice et al., Phys. Rev. A **22**, 310 (1980)

[13] E.Källne, J.Källne and R.D.Cowan, Phys. Rev. A **27**, 2682 (1983)

[14] P.Burkhalter et al., Phys. Rev. A **18**, 718 (1978)

[15] J.E.Rice and E.S.Marmar, Rev. Sci. Instrum. **61**, 2753 (1990)

[16] E.S.Marmar et al., Phys. Rev. A **33**, 774 (1986)

[17] G.W.Erickson, J. Phys. Chem. Ref. Data **6**, 831 (1977)

[18] V.A.Boiko et al., J. Phys. B **10**, 3387 (1977)

[19] L.A.Vainshtein and U.I.Safronova, Physica Scripta **31**, 519 (1985)

[20] J.F.Seely and U.Feldman, Phys. Rev. Lett. **54**, 1016 (1985)

[21] M.Klapisch, Comput. Phys. Commun. **2**, 269 (1971)

[22] M.Klapisch, J.L.Schwob, B.S.Fraenkel and J.Oreg, J. Opt. Soc. Am. **67**, 148 (1977)

[23] A.Bar-Shalom and M.Klapisch, Comput. Phys. Commun. **50**, 375 (1988)

[24] J.Oreg et al., Phys. Rev. A **44**, 3, 1741 (1991)

[25] J.Oreg, W.Goldstein and M.Klapisch, Phys. Rev. A **44**, 3, 1750 (1991)

[26] A.Bar-Shalom, M.Klapisch and J.Oreg, Phys. Rev. A **38**, 1773 (1988)

[27] R.D.Cowan, The Theory of Atomic Structure and Spectra, University of California Press, pp.433-434 (1981)

[28] P.Beiersdorfer, M.H.Chen, R.E.Marrs and M.Levine, Phys. Rev. A **41**, 3453 (1990)

[29] J.E.Rice, E.S.Marmar, E.Källne and J.Källne, Phys. Rev. A **35**, 3033 (1987)

[30] R.K.Janev et al., Phys. Rev. A **28**, 1293 (1983)

[31] M.Finkenthal et al., Phys. Rev. A **39**, 3717 (1989)

Table Captions

Table I Calibration lines from Ar^{16+} and Ar^{17+}.

Table II Calibration lines from Cl^{15+} and Cl^{16+}.

Table III The *j-j* wave function components of the Mo^{32+} $2p^5 6d$ and $2p^5 8d$ J=1 physical states. The coincidental overlap of the $(2p^5)_{\frac{1}{2}}nd$ and the $(2p^5)_{\frac{3}{2}}n'd$ ($n' > n$) orbitals in energy leads to the configuration interaction.

Table IV Mo^{30+} ($2p^6 3s^2$ ground state) resonance transitions. The column labeled 'upper state' shows the 2p hole, the spectator electron in braces and the occupied nd or ns orbital.

Table V Mo^{31+} ($2p^6 3s$ ground state) resonance transitions. The column labeled $\overline{\lambda}$ is the oscillator strength weighted average of the transition wavelengths for different transitions, close in energy, from the same configuration. The $\Delta\lambda$ values followed by asterisks are found by subtracting the measured transition wavelengths from the values of $\overline{\lambda}$. The column labeled 'upper state' shows the 2p hole, the spectator electron in braces and the occupied nd or ns orbital. Note the transitions with the 3p+ spectator end on the $2p^6 3p$ J=$\frac{3}{2}$ level. These lines (3787.4 mÅ) are not true resonance lines since the spectator electron is not in the 3s level.

Table VI Mo^{32+} ($2p^6$ ground state) resonance transitions. The column labeled 'upper state' shows the occupancy of the two relativistic 2p orbitals and the occupied upper orbital. In the case of a 2s-np transition, the numbers shown are the occupancy of the 2s orbital, the spectator electrons and the occupied upper orbital. The $(2p^5)_{\frac{3}{2}}$- $nd_{\frac{5}{2}}$ series limit is at 2914.78 mÅ, and the $(2p^5)_{\frac{1}{2}}$-$nd_{\frac{3}{2}}$ series limit is at 2841.44 mÅ.

Table VII Mo^{33+} ($2s^2 2p^5$ ground state) resonance transitions. The column labeled 'upper state' shows the occupancy of the two relativistic 2p orbitals and the occupied upper orbital. Transitions labeled with 'a' are to the $2s^2 2p^5$ J=$\frac{3}{2}$ true ground state, with 'b' are to the $2s^2 2p^5$ J=$\frac{1}{2}$ first excited state, and with 'c' are to the $2s2p^6$ second excited state. The line at 3269.7 mÅ has been identified

as a 2s-7p transition. However, it should be observed that the final state for this transition is the second excited state in Mo^{33+}, $2s2p^6$ $J=\frac{1}{2}$, and the only way the $2s2p^6$ - $2s^22p^47p$ decay takes place is that, in reality, there is a 2.75% admixture of the $2s2p^55d$ $J=\frac{1}{2}$ wave function in the $2s^22p^47p$ $J=\frac{1}{2}$ state. Thus, only through a 2p-5d dipole decay does the $2s^22p^47p$ state reach the $2s2p^6$ state.

Table I

Transition	wavelength (mÅ)	reference
$1s2p\ ^1P_1$ - $2p^2\ ^1D_2$	3771.79	16
$1s2s\ ^3S_1$ - $2s2p\ ^3P_2$	3761.06	16
$1s2s\ ^1S_0$ - $2s2p\ ^1P_1$	3755.26	16
$1s\ ^1S_{\frac{1}{2}}$ - $2p\ ^2P_{\frac{1}{2}}$	3736.52	17
$1s\ ^1S_{\frac{1}{2}}$ - $2p\ ^2P_{\frac{3}{2}}$	3731.10	17
$1s^2\ ^1S_0$ - $1s3p\ ^3P_1$	3369.61	18
$1s^2\ ^1S_0$ - $1s3p\ ^1P_1$	3365.71	19
$1s^2\ ^1S_0$ - $1s4p\ ^1P_1$	3199.77	19
$1s\ ^1S_{\frac{1}{2}}$ - $3p\ ^2P_{\frac{1}{2}}$	3151.38	17
$1s\ ^1S_{\frac{1}{2}}$ - $3p\ ^2P_{\frac{3}{2}}$	3150.24	17
$1s^2\ ^1S_0$ - $1s5p\ ^1P_1$	3128.47	20
$1s^2\ ^1S_0$ - $1s6p\ ^1P_1$	3090.91	20
$1s^2\ ^1S_0$ - $1s7p\ ^1P_1$	3068.70	20
$1s^2\ ^1S_0$ - $1s8p\ ^1P_1$	3054.43	20
$1s^2\ ^1S_0$ - $1s9p\ ^1P_1$	3045.06	20
$1s^2\ ^1S_0$ - $1s10p\ ^1P_1$	3037.51	20
$1s^2\ ^1S_0$ - $1s11p\ ^1P_1$	3032.75	20
$1s^2\ ^1S_0$ - $1s12p\ ^1P_1$	3028.90	20
$1s\ ^1S_{\frac{1}{2}}$ - $4p\ ^2P_{\frac{3}{2}}$	2987.34	17

Table II

Transition	wavelength (mÅ)	ref
$1s^2\ {}^1S_0$ - $1s3p\ {}^1P_1$	3789.89	19
$1s^2\ {}^1S_0$ - $1s4p\ {}^1P_1$	3603.56	19
$1s\ {}^1S_{\frac{1}{2}}$ - $3p\ {}^2P_{\frac{3}{2}}$	3533.49	17
$1s^2\ {}^1S_0$ - $1s5p\ {}^1P_1$	3523.35	19
$1s\ {}^1S_{\frac{1}{2}}$ - $4p\ {}^2P_{\frac{3}{2}}$	3350.71	17
$1s\ {}^1S_{\frac{1}{2}}$ - $5p\ {}^2P_{\frac{3}{2}}$	3272.36	17

Table III

Mo^{32+}
J=1, odd parity wavefunction purities (by RELAC)

physical states	$(2p^5)_{3/2}6d_{3/2}$	$(2p^5)_{1/2}6d_{3/2}$	$(2p^5)_{3/2}6d_{5/2}$	$(2p^5)_{3/2}7d_{3/2}$	$(2p^5)_{1/2}7d_{3/2}$	$(2p^5)_{3/2}7d_{5/2}$
$(2p^5)_{3/2}6d_{3/2}$	89.06	0.0	10.91	0.0	0.0	0.0
$(2p^5)_{1/2}6d_{3/2}$	0.0	82.52	0.02	5.85	0.01	11.36
$(2p^5)_{3/2}6d_{5/2}$	10.92	0.01	88.90	0.0	0.0	0.03

	$(2p^5)_{3/2}8d_{3/2}$	$(2p^5)_{1/2}8d_{3/2}$	$(2p^5)_{3/2}8_{5/2}$	$(2p^5)_{3/2}11d_{1/2}$	$(2p^5)_{1/2}11d_{3/2}$	$(2p^5)_{3/2}11d_{5/2}$
$(2p^5)_{3/2}8d_{3/2}$	89.12	0.0	10.86	0.0	0.0	0.0
$(2p^5)_{1/2}8d_{3/2}$	0.0	89.04	0.02	1.78	0.00	9.03
$(2p^5)_{3/2}8d_{5/2}$	10.87	0.0	89.00	0.0	0.0	0.0

Table IV

Mo^{30+} resonance transitions

transition	obser. λ(mÅ)	theor. λ(mÅ)	Δλ(mÅ)	g*f	upper state
2p-14d		3005.3		3.51E-03	2p-[3s^2]14d- J=1
2p-13d		3013.2		4.22E-03	2p-[3s^2]13d- J=1
2p-12d		3023.3		5.39E-03	2p-[3s^2]12d- J=1
2p-11d		3036.4		7.12E-03	2p-[3s^2]11d- J=1
2p-10d		3053.8		9.77E-03	2p-[3s^2]10d- J=1
2p-9d		3077.7		1.43E-02	2p-[3s^2]9d- J=1
2p-14d		3087.1		6.45E-03	2p+[3s^2]14d+ J=1
2p-13d		3095.5		8.14E-03	2p+[3s^2]13d+ J=1
2p-12d		3106.0		1.11E-02	2p+[3s^2]12d+ J=1
2p-8d		3111.8		2.05E-02	2p-[3s^2]8d- J=1
2p-11d		3119.8		1.28E-02	2p+[3s^2]11d+ J=1
2p-10d		3138.1		1.78E-02	2p+[3s^2]10d+ J=1
2p-7d		3160.4		5.91E-02	2p-[3s^2]7d- J=1
2p-9d		3161.8		5.31E-05	2p+[3s^2]9d+ J=1
2p-8d		3199.2		3.78E-02	2p+[3s^2]8d+ J=1
2s-5p		3206.3		3.74E-02	2s+[2p^{6}3s^2]5p+ J=1
2p-6d		3243.2		6.85E-02	2p-[3s^2]6d- J=1
2p-7d		3250.4		5.00E-02	2p+[3s^2]7d+ J=1
2p-6d		3337.5		1.10E-01	2p+[3s^2]6d+ J=1
2p-5d	3395.1	3395.4	0.3	1.03E-01	2p-[3s^2]5d- J=1

2p-5d	3497.0	3497.1	0.1	1.93E-01	$2p+[3s^2]5d+$ J=1
2s-4p		3507.2		1.11E-01	$2s+[2p^6 3s^2]4p+$ J=1
2p-4d	3715.5	3712.6	-2.9	2.86E-01	$2p-[3s^2]4d-$ J=1
2p-4s	3799.6	3800.1	0.5	2.67E-03	$2p-[3s^2]4s+$ J=1
2p-4d	3834.8	3831.6	-3.2	5.03E-01	$2p+[3s^2]4d+$ J=1

Table V

Mo^{31+} resonance transitions

transition	$\bar{\lambda}$(mÅ)	obser. λ(mÅ)	theor. λ(mÅ)	$\Delta\lambda$(mÅ)	g*f	upper state
2p-14d			2947.4		1.17E-03	2p-[3s+]14d- J=1/2
2p-14d			2947.4		1.37E-03	2p-[3s+]14d- J=3/2
2p-13d			2955.5		1.42E-03	2p-[3s+]13d- J=1/2
2p-13d			2957.1		1.06E-03	2p-[3s+]13d- J=3/2
2p-12d			2965.8		1.83E-03	2p-[3s+]12d- J=1/2
2p-12d			2965.8		2.09E-03	2p-[3s+]12d- J=3/2
2p-11d			2979.1		2.43E-03	2p-[3s+]11d- J=1/2
2p-11d			2980.7		1.62E-03	2p-[3s+]11d- J=3/2
2p-10d			2996.9		3.37E-03	2p-[3s+]10d- J=1/2
2p-10d			2996.9		3.77E-03	2p-[3s+]10d- J=3/2
2p-9d			3021.2		5.11E-03	2p-[3s+]9d- J=1/2
2p-9d			3021.3		5.48E-03	2p-[3s+]9d- J=3/2
2s-6p		3027.2	3027.4	0.2	6.58E-03	2s+[2p^{6}3s]6p+ J=3/2
2p-14d			3027.9		2.04E-03	2p+[3s+]14d+ J=3/2
2p-14d			3027.9		1.96E-03	2p+[3s+]14d+ J=1/2
2p-13d			3033.5		2.81E-03	2p+[3s+]13d+ J=3/2
2p-13d			3036.4		2.51E-03	2p+[3s+]13d+ J=1/2
2p-13d			3036.5		2.41E-03	2p+[3s+]13d+ J=3/2
2p-12d			3044.3		3.73E-03	2p+[3s+]12d+ J=3/2
2p-12d	3047.3	3047.4	3047.2	-0.1 *	3.25E-03	2p+[3s+]12d+ J=1/2
2p-12d	3047.3	3047.4	3047.3	-0.1 *	3.06E-03	2p+[3s+]12d+ J=3/2
2p-8d			3055.7		1.42E-03	2p-[3s+]8d- J=1/2
2p-8d			3055.8		1.78E-02	2p-[3s+]8d- J=3/2
2p-11d	3060.2	3060.1	3058.4	0.1 *	5.05E-03	2p+[3s+]11d+ J=3/2
2p-11d	3060.2	3060.1	3061.3	0.1 *	4.41E-03	2p+[3s+]11d+ J=1/2
2p-11d	3060.2	3060.1	3061.3	0.1 *	3.97E-03	2p+[3s+]11d+ J=3/2
2p-10d	3078.8	3078.9	3077.0	-0.1 *	7.10E-03	2p+[3s+]10d+ J=3/2
2p-10d	3078.8	3078.9	3079.9	-0.1 *	5.50E-03	2p+[3s+]10d+ J=1/2
2p-10d	3078.8	3078.9	3080.1	-0.1 *	5.25E-03	2p+[3s+]10d+ J=3/2

2p-9d			3102.7		1.05E-02	2p+[3s+]9d+ J=3/2
2p-9d	3105.7	3105.3	3105.6	0.4 *	8.07E-03	2p+[3s+]9d+ J=1/2
2p-9d	3105.7	3105.3	3105.8	0.4 *	7.17E-03	2p+[3s+]9d+ J=3/2
2p-7d			3108.1		1.10E-02	2p-[3s+]7d- J=1/2
2p-7d			3108.2		1.29E-02	2p-[3s+]7d- J=3/2
2p-8d			3138.9		1.61E-02	2p+[3s+]8d+ J=3/2
2p-8d	3141.9	3141.8	3141.8	0.1 *	1.21E-02	2p+[3s+]8d+ J=1/2
2p-8d	3141.9	3141.8	3142.0	0.1 *	1.03E-02	2p+[3s+]8d+ J=3/2
2s-5p			3169.9		1.86E-02	2s+[2p^{6}3s]5p+ J=3
2p-6d			3192.6		5.16E-02	2p-[3s+]6d- J=1/2
2p-6d			3192.9		3.44E-02	2p-[3s+]6d- J=3/2
2p-7d		3194.3	3194.2	-0.1	2.10E-02	2p+[3s+]7d+ J=3/2
2p-7d			3197.1		2.35E-02	2p+[3s+]7d+ J=1/2
2p-7d			3197.4		2.07E-02	2p+[3s+]7d+ J=3/2
2p-6d			3283.2		5.43E-02	2p+[3s+]6d+ J=3/2
2p-6d		3285.9	3286.1	0.2	2.66E-02	2p+[3s+]6d+ J=1/2
2p-6d			3288.5		3.28E-02	2p+[3s+]6d+ J=3/2
2p-5d	3344.9	3344.9	3344.7	0.0 *	3.55E-02	2p-[3s+]5d- J=1/2
2p-5d	3344.9	3344.9	3345.2	0.0 *	3.36E-02	2p-[3s+]5d- J=3/2
2p-5d		3442.9	3443.2	0.3	1.15E-01	2p+[3s+]5d+ J=3/2
2p-5d		3445.2	3445.4	0.2	5.99E-02	2p+[3s+]5d+ J=1/2
2p-5d		3447.8	3447.9	0.1	2.04E-02	2p+[3s+]5d+ J=3/2
2s-4p			3474.3		4.13E-02	2s+[2p^{6}3s]4p+ J=1/2
2s-4p			3474.6		4.95E-02	2s+[2p^{6}3s]4p+ J=3/2
2p-4d		3670.6	3670.3	-0.3	9.38E-02	2p-[3s+]4d- J=1/2
2p-4d		3670.6	3670.3	-0.3	1.32E-01	2p-[3s+]4d- J=3/2
2p-4s		3759.0	3758.7	-0.3	2.00E-03	2p-[3s+]4s+ J=3/2
2p-4d		3785.7	3786.2	0.5	3.07E-01	2p+[3s+]4d+ J=3/2
2p-4d (3p)+		3787.4	3787.9	0.5	8.18E-02	2p+[3p+]4d+ J=3/2
2p-4d (3p)+		3787.4	3787.9	0.5	1.19E-01	2p+[3p+]4d+ J=1/2
2p-4d			3789.4		1.51E-01	2p+[3s+]4d+ J=1/2

Table VI

Mo^{32+} resonance transitions

transition	obser. λ(mÅ)	theor. λ(mÅ)	Δλ(mÅ)	g*f	upper state
2p-14d		2891.1		7.07E-03	$(2p-)(2p+)^4 14d-$ J=1
2p-13d		2899.3		6.44E-03	$(2p-)(2p+)^4 13d-$ J=1
2p-12d		2909.8		7.45E-03	$(2p-)(2p+)^4 12d-$ J=1
2p-11d		2923.4		9.40E-03	$(2p-)(2p+)^4 11d-$ J=1
2p-10d		2941.4		1.27E-02	$(2p-)(2p+)^4 10-$ J=1
2p-9d		2966.2		2.42E-02	$(2p-)(2p+)^4 9d-$ J=1
2p-14d		2967.0		7.90E-03	$(2p-)^2(2p+)^3 14d+$ J=1
2p-13d	2976.1	2975.6	-0.5	1.19E-02	$(2p-)^2(2p+)^3 13d+$ J=1
2p-13s	2977.8	2977.1	-0.7	1.04E-03	$(2p-)^2(2p+)^3 13s+$ J=1
2s-6p		2980.2		2.49E-02	$2s+[2p^6]6p+$ J=1
2s-6p	2982.3	2982.3	0.0	9.79E-03	$2s+[2p^6]6p-$ J=1
2p-12d	2986.4	2986.6	0.2	1.40E-02	$(2p-)^2(2p+)^3 12d+$ J=1
2p-11d	3000.9	† 3000.9	0.0	4.19E-02	$(2p-)^2(2p+)^3 11d+$ J=1
2p-8d	3000.9	† 3001.3	0.4	1.08E-02	$(2p-)(2p+)^4 8d-$ J=1
2p-10d	3019.8	3020.3	0.5	2.36E-02	$(2p-)^2(2p+)^3 10d+$ J=1
2p-9d	3045.6	3045.9	0.3	3.44E-02	$(2p-)^2(2p+)^3 9d+$ J=1
2p-7d	3054.9	3054.6	-0.3	3.81E-02	$(2p-)(2p+)^4 7d-$ J=1
2p-8d	3083.1	3082.7	-0.4	5.11E-02	$(2p-)^2(2p+)^3 8d+$ J=1
2s-5p		3124.8		4.31E-02	$2s+[2p^6]5p+$ J=1
2s-5p		3129.4		1.62E-02	$2s+[2p^6]5p-$ J=1

2p-7d	3138.5	3138.4	-0.1	1.13E-01	$(2p-)^2(2p+)^3 7d+$ J=1
2p-6d		3142.5		1.97E-02	$(2p-)(2p+)^4 6d-$ J=1
2p-6d	3230.1	3230.6	0.5	1.19E-01	$(2p-)^2(2p+)^3 6d+$ J=1
2p-5d	3295.8	3295.5	-0.3	1.11E-01	$(2p-)(2p+)^4 5d-$ J=1
2p-5d	3392.0	3391.7	-0.3	2.14E-01	$(2p-)^2(2p+)^3 5d+$ J=1
2s-4p	3439.2	3437.7	-1.5	1.09E-01	$2s+[2p^6]4p+$ J=1
2s-4p	3450.7	3449.3	-1.4	4.45E-02	$2s+[2p^6]4p-$ J=1
2p-4d	3626.1	3626.1	0.0	3.02E-01	$(2p-)(2p+)^4 4d-$ J=1
2p-4d	3739.8	3739.8	0.0	5.17E-01	$(2p-)^2(2p+)^3 4d+$ J=1
2p-4s	3831.7	3831.6	-0.1	2.40E-02	$(2p-)^2(2p+)^3 4s+$ J=1

† The nearness of transition wavelengths makes these transitions unresolvable.

Table VII

Mo^{33+} resonance transitions

transition	obser. λ(mÅ)	theor. λ(mÅ)	Δλ(mÅ)	g*f	upper state
2p-8d a		2883.8 blend		4.04E-03 4.50E-03	$(2p-)(2p+)^3(8d-)$ J=5/2 + $(2p-)(2p+)^3(8d-)$ J=3/2
2p-8d a		2883.9		2.90E-03	$(2p-)(2p+)^3(8d-)$ J=1/2
2p-8d a		2894.1		4.76E-03	$(2p-)(2p+)^3(8d-)$ J=5/2
2p-7d a		2936.1 blend		6.43E-03 6.09E-03	$(2p-)(2p+)^3(7d-)$ J=5/2 + $(2p-)(2p+)^3(7d-)$ J=3/2
2p-7d a		2936.2		4.44E-03	$(2p-)(2p+)^3(7d-)$ J=1/2
2p-7d a		2946.7		1.02E-02	$(2p-)(2p+)^3(7d-)$ J=5/2
2p-8d a		2967.1		1.38E-01	$(2p-)^2(2p+)^2(8d+)$ J=5/2
2p-6d b	3012.6	3013.1	0.5	4.01E-02	$(2p+)^4(6d-)$ J=3/2
2p-6d a		3020.5		1.79E-02	$(2p-)(2p+)^3(6d-)$ J=5/2
2p-7d a	3022.3	3022.3	0.0	1.82E-02	$(2p-)^2(2p+)^2(7d+)$ J=5/2
2p-7d a		3022.5		9.19E-03	$(2p-)^2(2p+)^2(7d+)$ J=3/2
2p-6d a		3032.0		1.06E-02	$(2p-)(2p+)^3(6d-)$ J=5/2
2s-5p a		3047.1		9.96E-03	$(2s+)[2p^5](5p+)$ J=5/2
2s-5p a		3047.5		1.25E-02	$(2s+)[2p^5](5p+)$ J=3/2
2p-6d a	3111.6	3111.3	-0.3	3.81E-02	$(2p-)^2(2p+)^2(6d+)$ J=5/2
2p-5d a		3172.7		2.38E-02	$(2p-)(2p+)^3(5d-)$ J=5/2
2p-5d a		3172.8		2.34E-02	$(2p-)(2p+)^3(5d-)$ J=3/2
2p-5d a	3253.4	3252.4	-1.0	3.27E-03	$(2p-)^2(2p+)^2(5d-)$ J=3/2
2p-5d b	3261.0	3261.6	0.6	6.48E-02	$(2p-)(2p+)^3(5d+)$ J=1/2
2s-7p c	3269.7	† 3269.8	0.1	3.13E-03	$(2p-)^2(2p+)^2(7p+)$ J=3/2 + $(2s)[2p^5](5d+)$ J=3/2
2p-5d a		3271.5		7.09E-02	$(2p-)^2(2p+)^2(5d+)$ J=5/2
2s-4p a		3359.0		2.25E-02	$(2s+)[2p^5](4p+)$ J=5/2

2s-4p a		3359.7		2.56E-02	$(2s+)[2p^5](4p+)$ J=3/2
2s-4p a		3370.6		2.26E-02	$(2s+)[2p^5](4p-)$ J=5/2
2p-4d a	3498.0	3497.9	-0.1	7.31E-02	$(2p-)(2p+)^3(4d-)$ J=5/2
2p-4d a		3498.3		6.73E-02	$(2p-)(2p+)^3(4d-)$ J=3/2
2p-4d a	3513.1	3513.6	0.5	6.45E-02	$(2p-)(2p+)^3(4d-)$ J=5/2
2p-4d a		3592.1		6.69E-02	$(2p-)^2(2p+)^2(4d+)$ J=5/2
2p-4d b	3603.2	3602.6	-0.6	1.72E-01	$(2p-)(2p+)^3(4d+)$ J=1/2
2p-4d b	3604.3	3604.6	0.3	2.32E-01	$(2p-)(2p+)^3(4d+)$ J=3/2
2p-4d a	3615.3	3615.1	-0.2	1.68E-01	$(2p-)^2(2p+)^2(4d+)$ J=5/2
2p-4d a		3616.1		9.87E-02	$(2p-)^2(2p+)^2(4d+)$ J=3/2
2p-4d a	3619.8	3619.5	-0.3	2.56E-02	$(2p-)^2(2p+)^2(4d+)$ J=1/2
2p-4d b	3622.6	3622.2	-0.4	9.59E-02	$(2p-)(2p+)^3(4d+)$ J=3/2
2p-4s b	3682.1	3681.7	-0.4	1.46E-02	$(2p-)(2p+)^3(4s+)$ J=3/2
2p-4s a	3696.2	3695.7	-0.5	2.10E-03	$(2p-)^2(2p+)^2(4s+)$ J=5/2
2p-4d b	3717.8	3715.5	-2.3	9.18E-02	$(2p-)^2(2p+)^2(4d-)$ J=3/2

† Transition is allowed only through configuration mixing.

Figure Captions

Fig. 1 2p-4d transitions in Mo^{32+}, Mo^{31+} and Mo^{30+}. Theoretical lines for Mo^{32+} (solid), Mo^{31+} (dotted), Mo^{30+} (dash-dot-dash), Ar^{17+} (dashed) and Cl^{15+} (dash-dot-dot-dot-dash) are shown at the bottom.

Fig. 2 2p-4d transitions in Mo^{32+}, Mo^{31+} and Mo^{33+}. Theoretical lines for Mo^{32+} (solid), Mo^{31+} (dotted), Mo^{33+} (dashed) and Cl^{15+} (dash-dot-dot-dot-dash) are shown at the bottom.

Fig. 3 2p-5d transitions in Mo^{32+} (solid), Mo^{31+} (dotted) and Mo^{30+} (dash-dot-dash), and 2s-4p transitions in Mo^{32+} (solid).

Fig. 4 $2p_{\frac{3}{2}}$ - $nd_{\frac{5}{2}}$ transitions with $8 \leq n \leq 13$ in Mo^{32+}. Theoretical lines for Mo^{32+} (solid), Mo^{31+} (dotted), and Mo^{33+} (dashed) are shown at the bottom.

Fig. 5 gf values for $2p_{\frac{3}{2}}$-$nd_{\frac{5}{2}}$ (asterisks) and $2p_{\frac{1}{2}}$-$nd_{\frac{3}{2}}$ (plus signs) transitions in Mo^{32+} as a function of upper level principal quantum number n. Curves are proportional to n^{-3}.

Fig. 6 $2p_{\frac{3}{2}}$ - $7d_{\frac{5}{2}}$ transition in Mo^{32+}. Theoretical lines for Mo^{32+} (solid), Mo^{31+} (dotted), Ar^{16+} and Ar^{17+} (dash-dot-dot-dot-dash) are shown at the bottom.

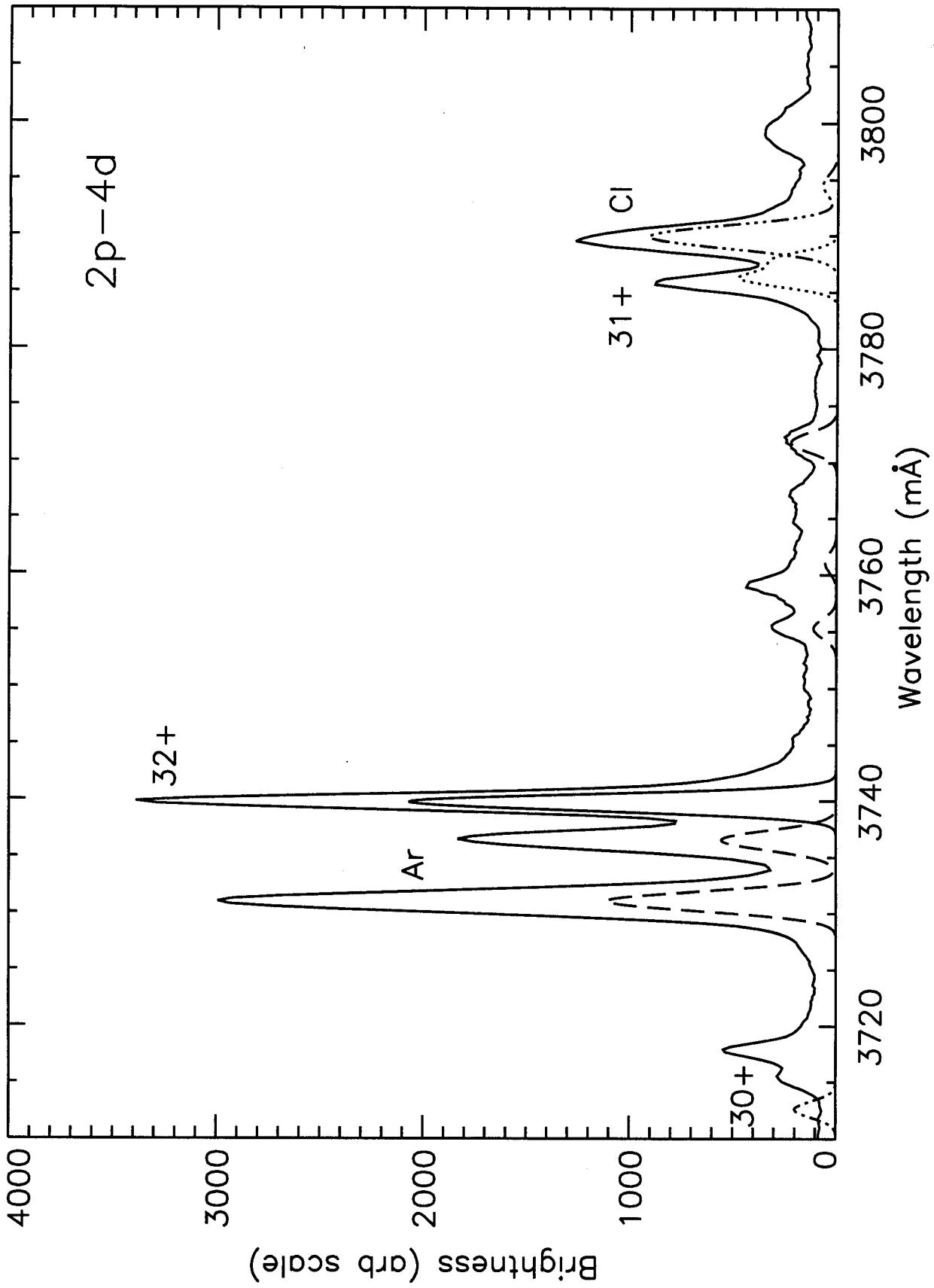
2p−4d
32+
Ar
30+
31+
Cl
Brightness (arb scale)
Wavelength (mÅ)
0
1000
2000
3000
4000
3720
3740
3760
3780
3800

Figure 1

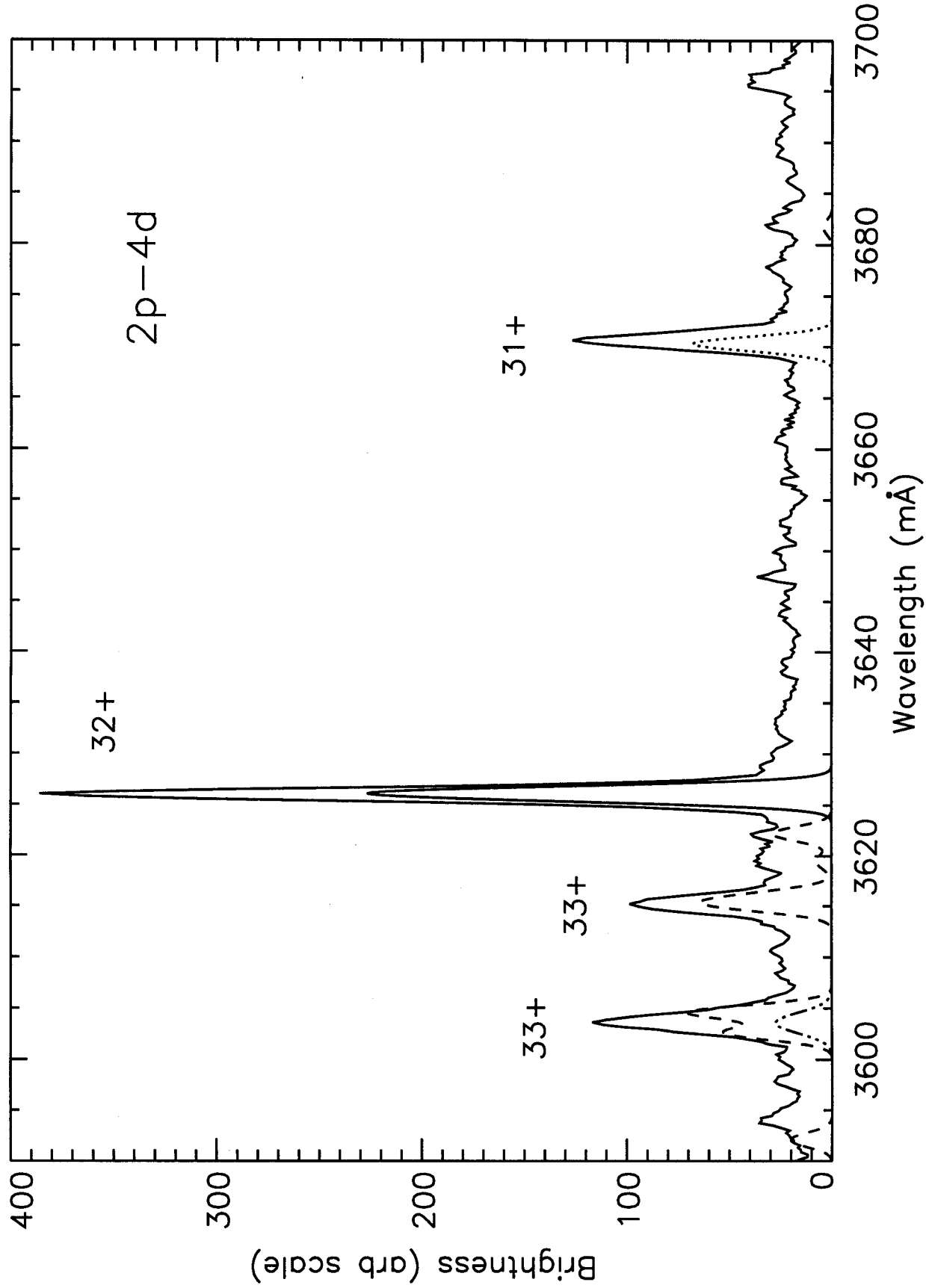
2p−4d
32+
31+
33+
33+
Brightness (arb scale)
Wavelength (mÅ)
0
100
200
300
400
3600
3620
3640
3660
3680
3700

Figure 2

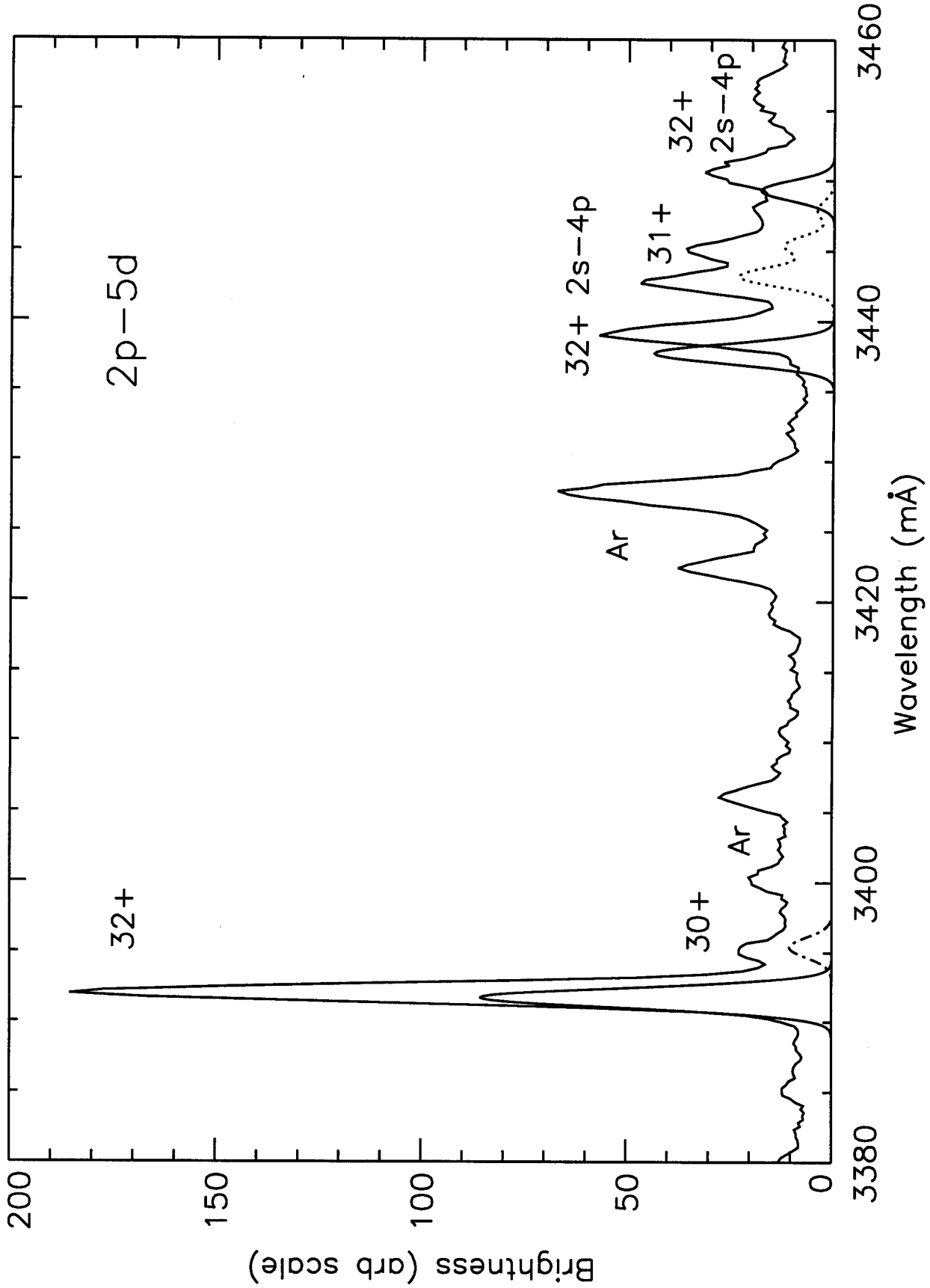
2p−5d
32+
30+
Ar
Ar
32+ 2s−4p
31+
32+
2s−4p
Brightness (arb scale)
Wavelength (mÅ)
0
50
100
150
200
3380
3400
3420
3440
3460

Figure 3

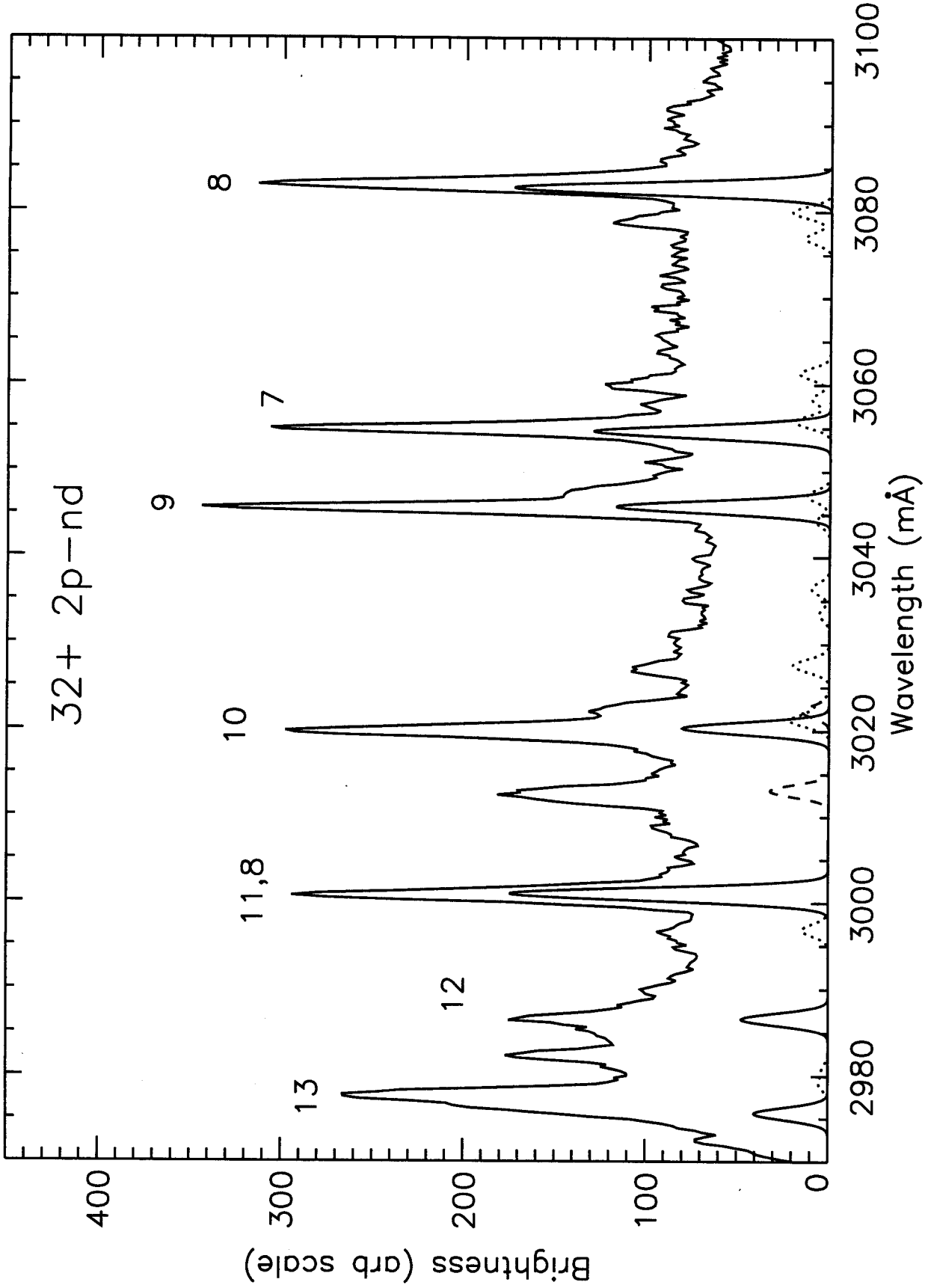
32+ 2p−nd
13
12
11,8
10
9
7
8
Brightness (arb scale)
0
100
200
300
400
2980
3000
3020
3040
3060
3080
3100
Wavelength (mÅ)

Figure 4

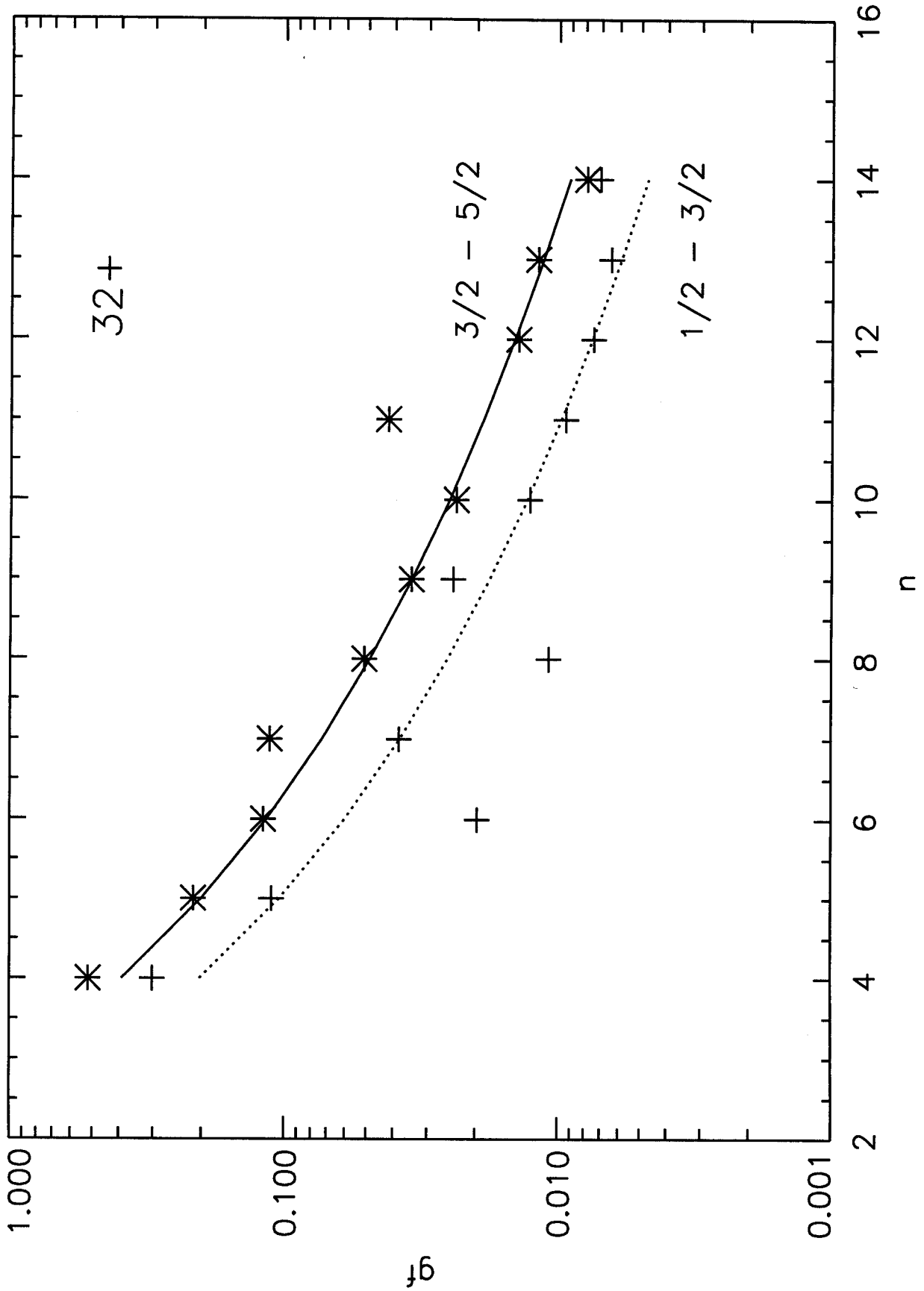

Figure 5

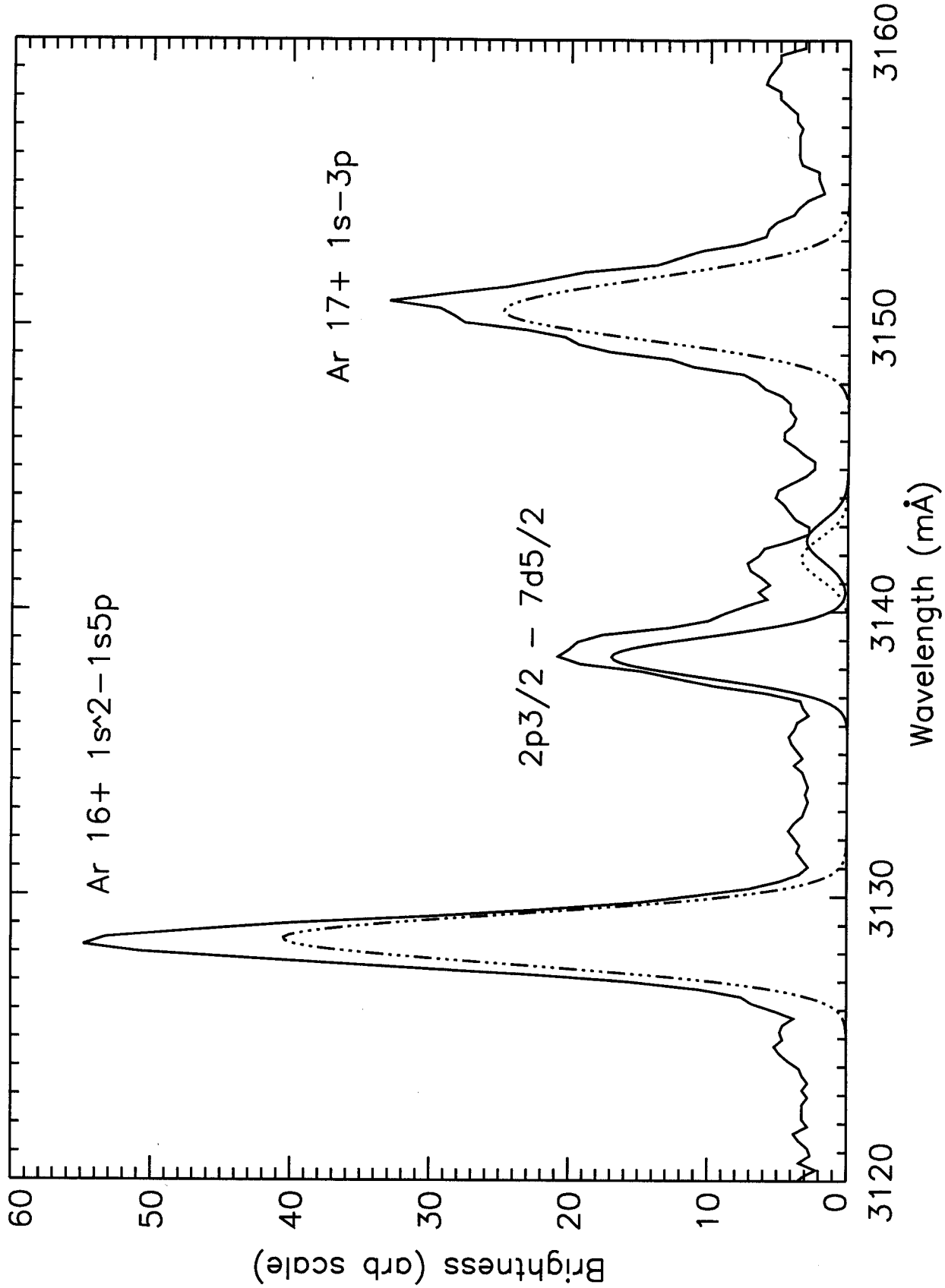
Brightness (arb scale)
Wavelength (mÅ)
Ar 16+ 1s^2−1s5p
Ar 17+ 1s−3p
2p3/2 − 7d5/2
0
10
20
30
40
50
60
3120
3130
3140
3150
3160

Figure 6